JOURNAL OF GEOPHYSICAL RESEARCH, VOL. 87, NO. A8, PAGES 6060–6072, AUGUST 1, 1982

Lion Roars and Nonoscillatory Drift Mirror Waves in the Magnetosheath

B. T. TSURUTANI,[1] E. J. SMITH,[1] R. R. ANDERSON,[2] K. W. OGILVIE,[3] J. D. SCUDDER,[3] D. N. BAKER,[4] AND S. J. BAME[4]

A complete set of ISEE plasma wave, plasma, and field data are used to identify the plasma instability responsible for the generation of extremely low frequency (ELF) electromagnetic lion roars. Lion roars detected close to the magnetopause are generated by the cyclotron instability of anisotropic ($T_\perp^-/T_\parallel^- \simeq 1.2$) thermal electrons when the local plasma critical energy, $E_M = B^2/8\pi N$, falls to values ($E_M \sim$ 10–30 eV) close to or below the electron thermal energy, 25 eV, as a result of decreases in B. A companion theoretical paper, Thorne and Tsurutani (1981), demonstrates that the convective growth rates of lion roars under these conditions is greater than 100 dB R_E^{-1}. The lion roars are terminated by increases in the ambient magnetic field magnitude and consequential increases in E_M to values greater than 100 eV. Because there are few resonant particles at these high energies, the growth rate decreases by 3 orders of magnitude and measurable growth ceases. The value of the absolute upper limit of the frequency of unstable waves predicted by theory, $\omega_{max} = A^-\Omega^-/(A^- + 1)$, is compared with observations. The predictions and observations are found to be in general, but not exact, agreement. Several possible explanations are explored. The quasi-periodic, ~20-s magnetic and plasma oscillations which cause the variations in E_M and hence alternately drive the cyclotron waves unstable and then stable are also investigated. The plasma and field pressures are shown to be out of phase, while the total pressure (electron + ion + field) remains relatively constant. Most of the pressure is associated with the particle thermal motion. The large 2:1 variations in field strength cause large oscillations in β ($8\pi P/B^2$), from β = 1–2 at field maximum to β = 10–25 at field minimum. Analysis of the high-resolution magnetic fields at the two closely separated spacecraft, ISEE 1 and 2, rule out the possibility that these field and plasma oscillations could be due to magnetopause motion. Cross-correlation analyses of the magnetic fields at the two spacecraft and the time delays for maximum correlation are shown to be consistent with the magnetic structures being quasi-static in nature. The temporal variations of the plasma and fields are due to spatial structures convecting past the spacecraft at the magnetosheath flow speed. The quasi-periodic structures are ~20 proton gyroradii in scale in the plasma rest frame. Magnetic structures with similar scale lengths are also shown to exist in the magnetosheaths of Jupiter and Saturn (Pioneer 11 data). The results are consistent with the interpretation that these magnetohydrodynamic structures are nonoscillatory 'waves' generated by the drift mirror instability. The condition for instability, $\beta_\perp/\beta_\parallel > 1 + (1/\beta_\perp)$, is met for the cases studied in this paper. The electron and ion instabilities are intimately coupled. The generation of high β (>10), low critical energy (E_M = 10–30 eV) regions by the drift mirror instability leads to the electrons becoming cyclotron unstable. The consequential whistler mode lion roars can then be ducted by the enhanced-density, low-field regions. Thus lion roar durations may not represent the propagation time for an electromagnetic wave packet travelling at the group velocity, but may correspond to the convection of a magnetosheath duct (drift mirror wave) past the spacecraft. The cyclotron and drift mirror instabilities occurring in the magnetosheath are natural relaxation processes that reduce the plasma pressure anisotropies created by preferential heating of the solar wind plasma as it passes through the bow shock and the further compression that takes place as the plasma and fields approach the near-subsolar magnetopause. One consequence of the onset of the instabilities and isotropization of the plasma is the enhanced expulsion of the plasma along field lines toward the flanks of the magnetosheath. It remains to be determined if this mechanism is a general process of 'plasma removal' from planetary magnetosheaths. Furthermore, the presence of nonoscillatory drift mirror waves and the convection of these structures to the magnetopause may have important consequences for magnetic merging. The alternating high and low β regions and the ($T_\perp > T_\parallel$) plasma temperature anisotropies may lead to patchy, sporadic reconnection.

1. INTRODUCTION

Lion roars are intense bursts of electromagnetic waves which are detected throughout the hot magnetosheath plasma [*Smith et al.*, 1969, 1971]. The emissions have a mean frequency of ~100 Hz (0.25–0.5 Ω^-), typical amplitude of 0.1 nT, and an average burst duration of 1–2 s [*Smith and Tsurutani*, 1976]. When played through a loudspeaker, the low-frequency, intense emissions sound like a roaring lion, hence the name [*Smith et al.*, 1971]. Lion roars are the most intense whistler mode emissions detected in the magnetosheath, and as such, the determination of the responsible instability is of interest from the standpoint of basic plasma physics, wave-particle interactions, and magnetosheath dynamics.

In a previous study [*Smith and Tsurutani*, 1976], lion roars were shown to be right-hand circularly polarized whistler mode waves, having the same sense of rotation as electrons gyrating about the magnetic field. The waves propagate essentially parallel (<15°) to the ambient magnetic field. A characteristic feature of the emissions is that, in some

[1] Jet Propulsion Laboratory, California Institute of Technology, Pasadena, California 91109.
[2] The University of Iowa, Iowa City, Iowa 52242.
[3] NASA Goddard Space Flight Center, Greenbelt, Maryland 20771.
[4] Los Alamos National Laboratory, Los Alamos, New Mexico 87545.

Paper number 2A0659.
0148-0227/82/002A-0659$05.00

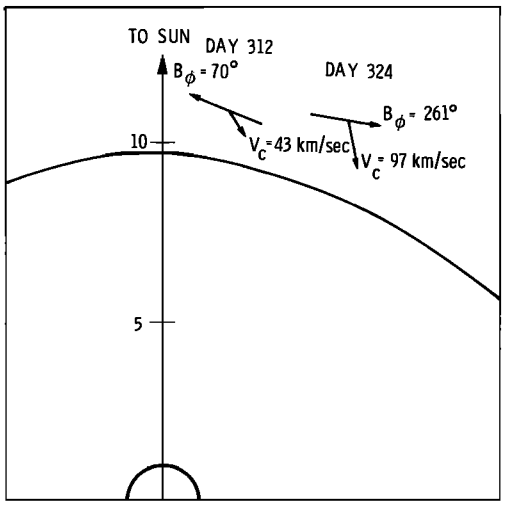

Fig. 1. The ISEE spacecraft positions relative to earth, the magnetosheath magnetic field directions, and the plasma convection flows for the events on days 312 and 324, 1977. For both events the ISEE spacecraft were in the magnetosheath just outside the magnetosphere. On day 312, ISEE 1 and 2 were at 11.8 R_E and a local time of 1120, and for day 324, 12.4 R_E and a local time of 1020. The magnetic fields are approximately parallel to the magnetopause, an orientation consistent with field line draping around the magnetosphere [*Fairfield*, 1967].

intervals, they exhibit excellent correlations with decreases in the magnetic field magnitude. During intervals when such correlations occur, field depressions are present for essentially each and every lion roar detected.

The observed wave properties place stringent requirements on possible instabilities generating the emissions. Landau resonance with either electrons or protons can be excluded because the waves propagate along the magnetic field, indicating the absence of a substantial electric field component of the wave parallel to **B**, a necessary condition for the (Landau) interaction to occur. Doppler-shifted cyclotron resonance with electrons has been mentioned as a possible generation mechanism [*Smith and Tsurutani*, 1976]. In the flanks of the magnetosheath, for a typical field strength of 10 nT and particle density of 10 cm^{-3}, the parallel kinetic energy of the resonant electrons would be ~18 eV. A typical magnetosheath electron temperature of ~3 × 10^5 K indicates the width of the electron distribution (~26 eV) is slightly greater than the above resonant energy; thus the latter would be near the most probable speed of the distribution function. Because there are copious numbers of resonant electrons (essentially the bulk of the plasma) involved in this possible instability, small anisotropies can give rise to very large wave growth and intensities. Another possible mechanism is generation by a cyclotron overstability caused by field-aligned streaming of ≅10-keV magnetosheath protons [*Smith and Tsurutani*, 1976].

This article has two main purposes. First, a full complement of ISEE 1 plasma, plasma wave and magnetic field data will be studied to identify the instability responsible for the generation of ELF lion roars. Two events which occur when ISEE 1 is close to the magnetopause have been specifically selected for this purpose. The observations and analyses of these lion roar events are presented in section 2, and the conclusions and discussion are in section 3.

This paper will demonstrate that ELF lion roars are intimately coupled to quasi-periodic large-scale magnetosheath structures. The latter are waves generated by another (the drift mirror) instability. Thus a second goal of the paper will be to identify and describe the magnetic and plasma features associated with this instability. The observations and analyses of the large-scale structures using ISEE 1, 2 for the earth's magnetosheath and Pioneer 11 data for Jupiter and Saturn are presented in section 4. Section 5 contains the background for the drift mirror waves. The conclusions are

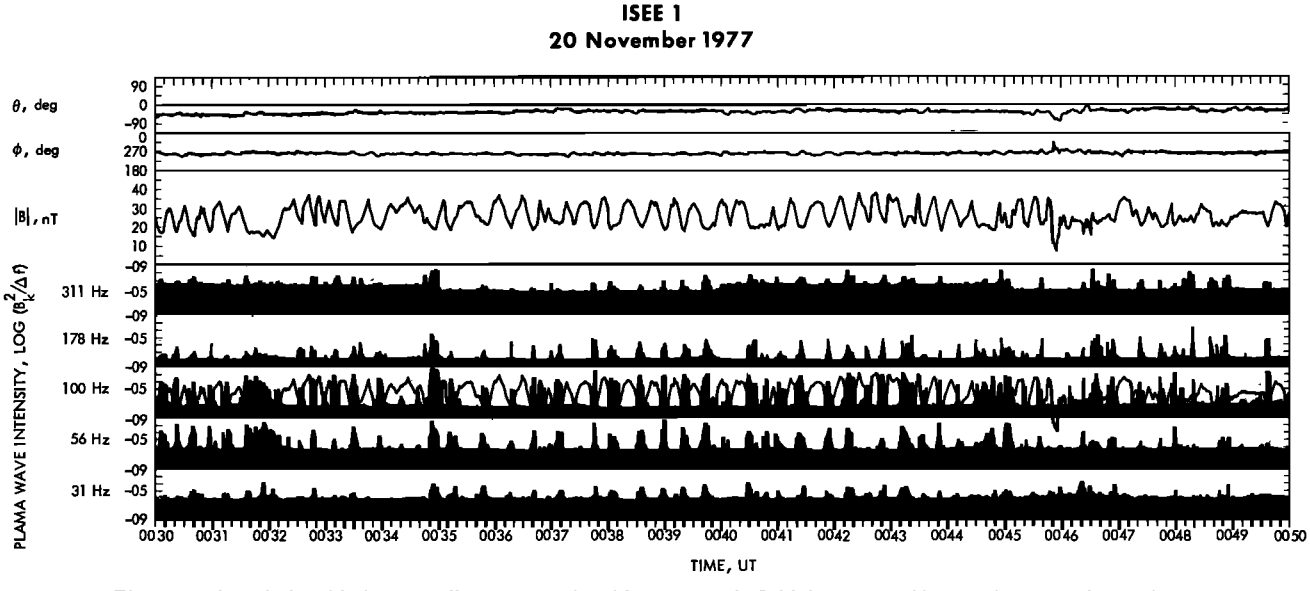

Fig. 2. The relationship between lion roars and ambient magnetic field decreases. The top three panels are the two field angles (in solar ecliptic coordinates) and the field magnitude. The lower panels are the intensities of the magnetic component of the plasma waves for five spectral channels. The dc magnetic field magnitude is replotted with the 100-Hz wave channel to illustrate the correlation between lion roars and field decreases. Within the interval shown, lion roars occur during each and every decrease in the field magnitude. The magnetic oscillations and the lion roars have temporal spacings of ~20 s. The magnetic field azimuthal angle ϕ is 261°, an orientation close to parallel to the magnetopause. The field angular changes are small in comparison with the large, 2-to-1 magnitude changes.

presented in section 6. Some further comments on the coupling between lion roars and drift mirror waves and the 'generality of the results' of this paper are given in section 7.

The ISEE 1 plasma, plasma wave, and magnetic field instruments are described in the work of *Bame et al.* [1978], *Ogilvie et al.* [1978], *Gurnett et al.* [1978], and *Russell* [1978]. The Pioneer 11 magnetic field instrument is discussed in the work of *Smith et al.* [1975].

2. Lion Roars: ISEE Observations and Analyses

Two somewhat unusual events were chosen for study, one because of a quasi-periodic spacing between the lion roars in the event (November 20, 1977) and the other (November 8, 1977) because the event contained long duration (~20 s) bursts. The latter property is necessary to obtain plasma measurements with time scales adequate to study the plasma properties prior to, during, and following the lion roar. Both of the above events were detected when the ISEE 1 and 2 spacecraft were very near the prenoon dayside magnetopause (1020 and 1120 local time, respectively). The locations of the ISEE spacecraft, the magnetic field orientations, and the magnetosheath plasma flow projections are depicted in Figure 1.

The relationship between the lion roars and the magnetosheath field is illustrated in Figure 2. The top three panels contain the magnetosheath magnetic field, represented as a field magnitude and two angles in the solar ecliptic (SE) coordinate system. The bottom five panels are the magnetic component of the plasma waves in various frequency bands. The vertical amplitude is the logarithm of the wave intensity. The spectral channels have bandwidths that are ±15% of the center frequencies. The field magnitude is superimposed on the 100-Hz channel of the wave plot to illustrate the detailed relationship between the lion roars and the field variations. During this event, ISEE 1 was located just beyond the magnetopause (which was crossed at 0053 UT), at 12.4 R_E and 1020 LT.

The lion roars are quasi-periodic, with a typical time interval of ~20 s between bursts. The emissions are broadband with peak intensities near, but below, 100 Hz. Their durations are somewhat longer than the nominal value of ~1–2 s found in the previous OGO 5 study [*Smith and Tsurutani*, 1976].

In the time interval from 0030 to 0045 UT, lion roars exhibit a one-to-one correlation with decreases in the ambient magnetic field. Each decrease in the magnetosheath field magnitude is accompanied by a lion roar. Conversely, lion roars are not detected at times other than during decreases in the magnetic field. Following this time interval, the quasi-periodic magnetic field variations disappear (beginning at 0045:50 UT). However, the correlation between magnetic field minima and the lion roars persists even in the absence of ordered field variations.

The magnetosheath magnetic field oscillations are very large, with ratios $\delta B/B$ as large as two to one. The magnetic variations are compressional, since the ϕ and θ field angles show little variation. The average field is parallel to the magnetopause but with a slight southward component. This orientation is consistent with field line 'draping' around the magnetosphere, as expected near the magnetopause [*Fairfield*, 1967].

Figure 3 illustrates the relationship between lion roars, the ambient magnetic field, and the plasma (proton) density. The proton density shown in the top panel is obtained from a measurement of the proton distribution function made every

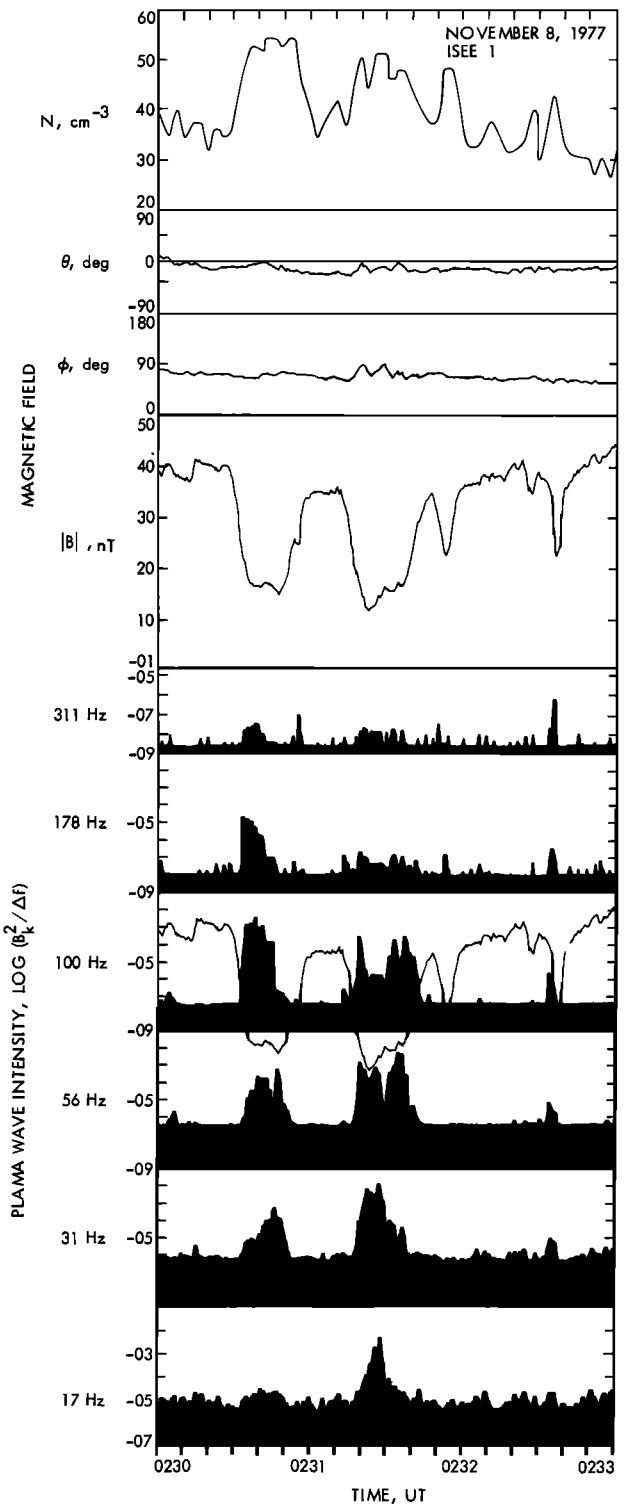

Fig. 3. The relationship among lion roars, the ambient magnetic field, and the plasma density, for day 312, 1977. The format is the same as in Figure 2, except the high-time resolution proton density is included at the top of the figure. Lion roars are again correlated with decreases in magnetic field. The proton density is anticorrelated with the magnetic field magnitude. The magnetic field orientation is approximately parallel to the magnetopause and remains relatively constant throughout the event.

3 s. At this high time resolution, ~7 density determinations are made during each of the long-duration lion roars. The bottom panels contain the same parameters as those in Figure 2. The ambient magnetic field is superimposed on top of the 100-Hz wave channel. ISEE 1 was located in the magnetosheath just beyond the magnetopause at 11.8 R_E and a local time of 1120.

The figure contains two intense lion roars at 0230:40 UT and 0231:25 UT and a smaller burst at 0232:35 UT. The peak intensity occurs just below 100 Hz for all three bursts. The bandwidths are relatively broad. The first emission does not extend to frequencies much below 31 Hz, but the waves are detectable at frequencies up to 562 Hz. The second large lion roar is limited to the frequency range from 17 Hz to about 100 Hz. The small burst at 0232:40 UT extends to frequencies beyond 311 Hz.

The three lion roars in the figures are correlated with decreases in the magnetic field intensity, in agreement with Figure 1 and with previous work [*Smith and Tsurutani*, 1976]. The primary difference between the above cases and the average magnetosheath events previously discussed is that the relative field decreases, $\delta B/B$, have values of 30–50%, considerably larger than the value of 10% reported in the earlier study.

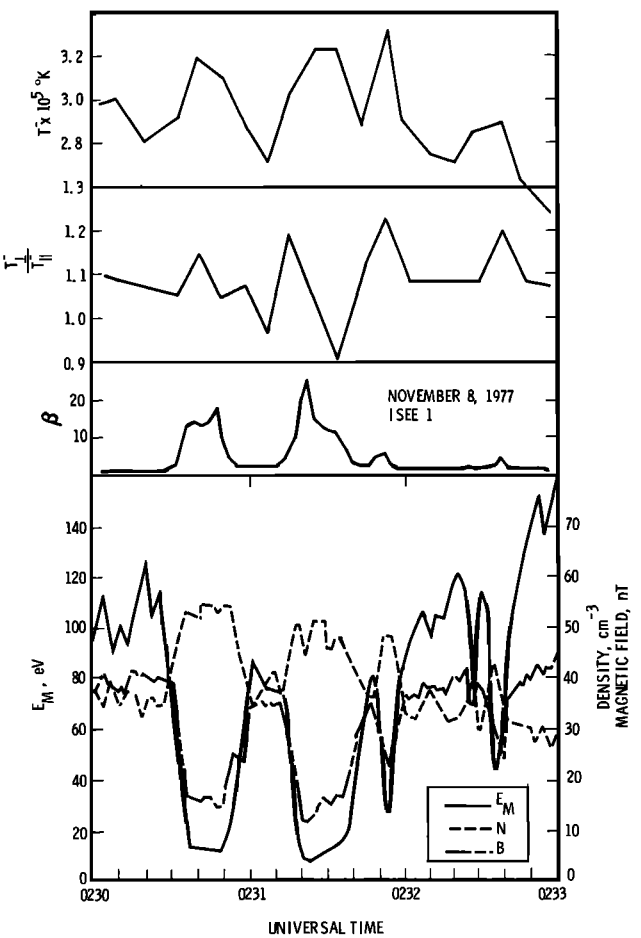

Fig. 4. Plasma parameters for the event in Figure 3. The electron average temperature and temperature anisotropy are given in the top two panels followed by the plasma β. The bottom panel contains the plasma density N, the magnetic field strength B, and the critical energy $E_M = B^2/8\pi N$. Lion roars occur in regions of high β (10–25), high temperature anisotropy ($T_\perp^-/T_\parallel^- \simeq 1.2$), high temperature ($T^- \simeq 3.2 \times 10^5$ K), and low critical energy (10–30 eV). The parallel energy for the resonant electrons, which is related to E_M, is near the electron thermal value (26 eV).

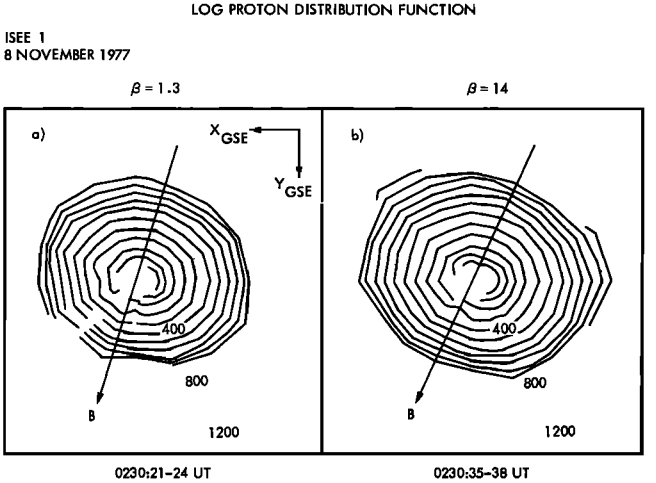

Fig. 5. Examples of the proton distribution function (*a*) in a low β region and (*b*) in a high β region. The β values can be obtained from Figure 4. A $T_\perp^+ > T_\parallel^+$ temperature anisotropy is present in both regions. Both parallel and perpendicular proton temperatures are greater in the high β regions. From the 25 distributions analyzed from 0230 to 0232 UT day 312, 1977, the temperature anisotropy range is $1.06 \leq T_\perp^+/T_\parallel^+ \leq 1.2$ and the temperature ($\bar{T} = (2T_\perp^+ + T_\parallel^+)/3$) is 5–10% greater inside the high β regions than outside.

The magnetic field variations are again found to be mainly compressional, with little change in the field direction. The average field is parallel to the magnetopause and lies in the ecliptic plane. The interplanetary sector polarity is opposite to that of the previous examples in Figure 2.

Plasma density enhancements occur simultaneously with each of the magnetic field decreases. The anticorrelation between density increases and field decreases is present for each of the three previously mentioned events plus a short-duration event at ~0231:55 UT.

The anticorrelation between the magnetic field intensity and the plasma density, and the large variations in the above quantities (particularly in the magnetic field), indicates that plasma parameters which are dependent on the ratio of B and N will vary greatly. The critical energy, $E_M = B^2/8\pi N$, and the plasma β, $8\pi NkT/B^2$, are shown in Figure 4 for the same time interval as in Figure 3. The magnetic field magnitude and density are repeated for reference. The β of the plasma is typically 1–2 in the high-magnetic field regions but increases to values >10 in the low-field regions. The critical energy E_M is 80–100 eV in the high-field regions but is an order of magnitude lower, a minimum of 10 eV during the two major field decreases. Thus the lion roars are detected in regions of very low critical energy (E_M = 10–40 eV) or, conversely, in high β (10–25) regions.

The electron temperature anisotropy is calculated from the model-free three-dimensional distribution function, determined by the ISEE vector electron spectrometer during a single spin. The temperatures and temperature anisotropies are illustrated in the top two panels of Figure 4. Average electron temperatures are ~3 × 10^5 K with maximum values of ~3.3 × 10^5 K detected in the high beta regions. Throughout this time interval, $T_\perp^-/T_\parallel^-$ is greater than unity (except for two points) and is also largest in the high β regions. The peak anisotropies are slightly greater than 1.2.

Examples of the proton two-dimensional contours of the log of the proton distribution function, $f(v)$, are given in Figure 5. Two contours per decade are plotted. The grid on each frame is scaled in a polar sense. The radial distance from the center is in units of kilometers per second. Each GSE x-y distribution is determined over a 3-s interval, the spacecraft spin period. For convenience, the solar direction is indicated, and the projection of the magnetic field into the x-y plane has been added to the figure.

Two contours have been selected as representative of the proton distribution function during the period 0230–0233 UT November 8, 1977 (see Figure 4 for reference). One distribution is observed during a low β region (Figure 5*a*) and the other during a high β lion roar period (Figure 5*b*).

Two outstanding features are readily apparent from Figure 5. A temperature anisotropy ($T_\perp{}^+ > T_\parallel{}^+$) is present in both the high and low β regions. Second, the proton temperature is greater in the high β region (determined from the magnitude of the radius of the contours). Both of these features are typical of the interval studied. The temperature anisotropy is found to remain within the limits of $1.06 \leq T_\perp{}^+/T_\parallel{}^+ \leq 1.2$. No evidence of >2 keV streaming protons was found in either this data or in the NOAA medium energy particle experiment data (D. J. Williams, personal communication, 1981). The proton temperature is consistently found to be larger within the high β regions. The magnitude of this variation is of the order of 5–10%, similar to that of the electron temperature variations.

The electron temperature and temperature anisotropy for other periods of day 312 and for day 324 have been studied. The results are consistent with those presented previously. A figure from *Anderson et al.* [1982], illustrating the relationship between lion roars and field decreases, is used to illustrate the dependences of the electron temperature and temperature anisotropy on the magnetic field strength (and β). This example from day 312 is shown as Figure 6. In the figure, $T_\perp{}^-/T_\parallel{}^-$ is greater than unity throughout the interval (except for two points). The largest anisotropies are generally detected in the high β regions. The maximum anisotropy measured is ~1.2. The electron temperature is highest in the high β regions and lowest in the high-field (low β) regions.

3. Lion Roars: Discussion

The analyses of a complementary set of plasma, plasma wave, and magnetic field data from ISEE 1 have provided the necessary information to identify the plasma instability responsible for the generation of lion roars. We have demonstrated that lion roars occur in regions of relative field

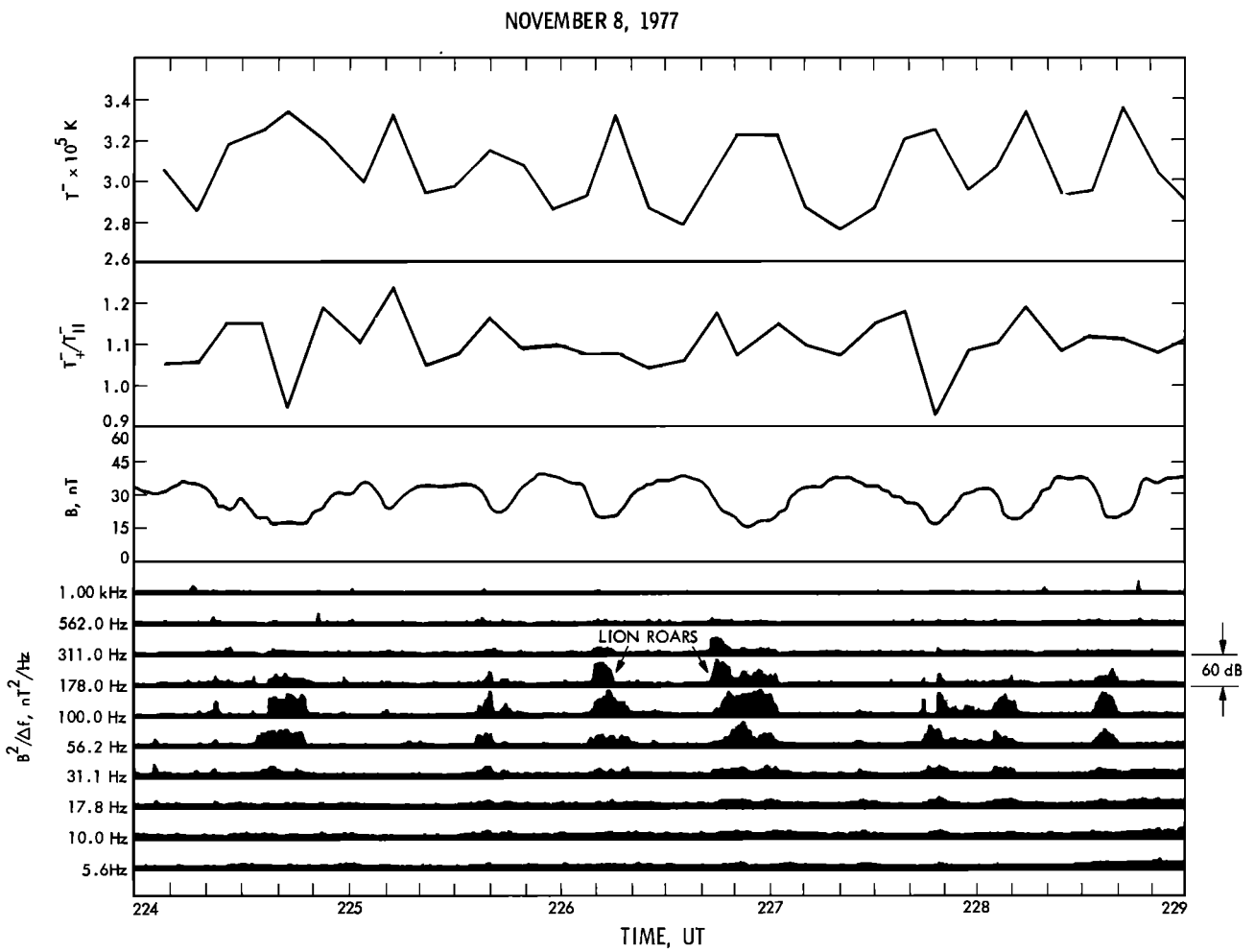

Fig. 6. A further example of the electron temperature and temperature anisotropy dependences on field decreases (high β regions). Lion roars occur in almost all of the field decreases (taken from *Anderson et al.* [1982]). The electron temperature anisotropy is generally greater than 1.0, with the largest values (up to 1.2) occurring in the minimum field regions. The electron temperatures are ~10% larger in the low-field (high β) regions.

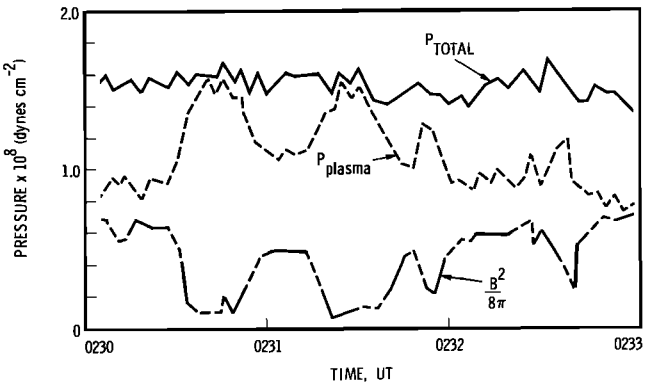

Fig. 7. The plasma, magnetic field, and total (plasma plus field) pressures, for the event in Figure 3. The total pressure is relatively constant throughout the time period, consistent with the variations being static structures convected by the magnetosheath plasma flow. The proton pressure anisotropy, $P_\perp^+/P_\parallel^+ \simeq 1.1$–$1.2$, is consistent with the structures being generated by the drift mirror instability.

minima (Figures 2, 3, 6, and *Smith and Tsurutani* [1976]) which are also regions of high β (Figure 4). The electron temperature anisotropy is largest within these regions, $T_\perp^-/T_\parallel^- \simeq 1.2$ (Figures 4, 6). Conversely, lion roars are not detected within the high magnetic field, relatively low β portions of the magnetosheath, even though the electron temperature anisotropy is greater than 1.0.

The above observations are consistent with the generation of lion roars by a cyclotron instability where the growth rate is controlled by the local plasma conditions. The variations in magnetic pressure, which are the principal cause of β variations from 1 to 25, effectively change the critical energy of the plasma from >100 eV to <15 eV. In a companion theoretical paper, *Thorne and Tsurutani* [1981] have used the above observations to demonstrate that the convection growth rate of lion roars in these high β regions is greater than 100 dB R_E^{-1} over a broad frequency range in agreement with the observations. The termination of lion roars with increasing field strength (low β regions) can be understood by noting that the critical energy (and the cyclotron resonant energy) increases to values well above the electron thermal energy, 26 eV. Because there are few resonant electrons present (the number decreases by 3 orders of magnitude in the lowest β regions), the wave growth is confined to a very narrow frequency band. Although a significant electron temperature anisotropy exists, the wave growth rate over a broad frequency range is well below 100 dB R_E^{-1} [*Thorne and Tsurutani*, 1981], thus explaining the observed lack of whistler mode emissions in these regions.

Linear theory [*Kennel and Petschek*, 1966] predicts an absolute upper limit to the frequency of unstable waves given by $(\omega/\Omega^-)_{max} = A^-/(1 + A^-)$. In the above expression, the pitch angle anisotropy A^-, is equal to $T_\perp^-/T_\parallel^- - 1$, and Ω^- is the electron cyclotron frequency. Using the maximum electron temperature anisotropy observed in Figure 4, a maximum lion roar frequency of $\simeq 0.2\Omega^-$ is implied. For a magnetic field of 20 nT, an upper frequency limit to the lion roars should be ~120 Hz. However, from Figure 3, it is clear that although the peak intensity is detected at a frequency below 100 Hz, components well above 120 Hz are present.

There are several possible causes for this lack of agreement between observation and linear theory. First, the electron temperatures are moments of an empirical distribution assumed to be unchanging (stationary) during the time of measurement. Deviations from constancy or an undetected portion of the electron distribution could cause an underestimation of the anisotropy. It is also possible that the waves have propagated from another region in the magnetosheath where plasma conditions are different. The plasma enhancements and field decreases in the high β regions can act as excellent wave guides, as we will discuss later in this paper. However, from an examination of numerous other cases on day 312 and 324, large temperature anisotropies were not detected, making this explanation unattractive. The third possibility is that nonlinear effects are important and that present theory is not adequate to explain all of the features of this instability.

4. Drift Mirror Waves: ISEE 1 and 2 Observations and Analyses

Figure 4 illustrates that the plasma (ion plus electron) pressure is 180° out of phase with the magnetic pressure in these MHD structures. The total pressure (gas plus magnetic) is constant across the oscillations (Figure 7). Other periods of November 8, 1977, were examined and similar results were obtained. Although the plasma data resolution is considerably reduced (lower data rates) on day 324, 1977, a comparison between the plasma and field also indicate a relationship consistent with the above.

The plasma temperature features illustrated in Figures 4, 5, and 6 can help identify the nature of the MHD structures. Both the electron temperature and the temperature anisotropy values are larger (by ~10%) in the regions where the plasma β is highest (Figures 4, 6). The proton temperature is largest in the high β regions, and $T_\perp^+$ is greater than $T_\parallel^+$ everywhere.

From the field and plasma parameters shown in Figure 4, it can easily be demonstrated that the high and low β regions

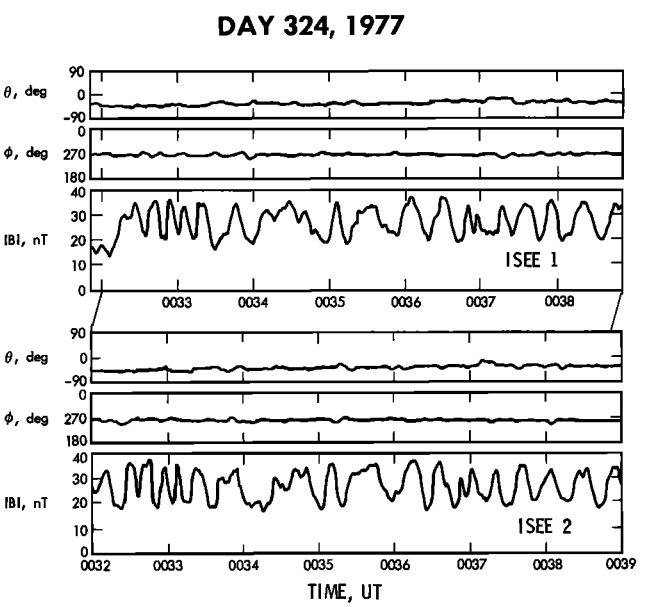

Fig. 8. Comparison of the magnetic fields at ISEE 1 and at ISEE 2 for day 324, 1977. The two data sets are offset by 5 s, as indicated by the time markers. The field is basically the same at the two spacecraft and is typical of the magnetosheath observations during this day. A peak-to-peak correlation is found in most instances. The quasi-period of the magnetic structures is ~20 s.

are adiabatically decoupled from one another. A representative field magnitude in the low β region is 40 nT and in the high β region, 15 nT. The ratio in the field strengths of the two regions is $\simeq$2.5. If the first adiabatic invariant, $\mu = kT_\perp/B$, is conserved, $T_\perp$ and B should change proportionately. In Figures 4 and 6 it was shown that the electron temperatures and temperature ratios are $\sim$10% less in the low β regions than in the high β regions. Thus $T_\perp^-$ increases by $\geq$10% in the high regions. The electron perpendicular kinetic energy does not vary with field strength, and thus μ is not constant across the MHD structures. In fact, the two parameters $T_\perp^-$ and B vary in the opposite sense. As B decreases, $kT_\perp^-$ increases. Similar arguments can be made for the protons.

Magnetopause Oscillations?

Figure 8 is a comparison of the magnetic field data from ISEE 1 and 2 for an interval in day 324. A transient change in the field direction occurs near 0046 UT at both spacecraft (not shown—see Figure 2 for ISEE 1), and this feature has been used to align the two data sets. A shift of 5 s in the ISEE 2 plot relative to ISEE 1 is necessary to achieve this alignment. Although the magnetic signatures are not exactly identical at the two spacecraft, an excellent correspondence exists between the two sets of measurements.

The magnetic field azimuth angle, ϕ, has an average value of 261° throughout the interval. With the spacecraft located at 1020 local time, this orientation corresponds to a 'draped' magnetosheath field. The magnetic field remains constant in direction as the magnitude varies by a factor of 2. No magnetospheric (θ = 90°, ϕ = 0°) field orientations are evident during this interval.

The nature of the field variations shown in the previous figures can be determined by comparing possible models with simultaneous ISEE 1 and ISEE 2 measurements. Several possible configurations are shown in Figure 9. The left-hand portion of the figure shows several possibilities and a time sequence of each, labeled a to e. The right-hand side represents the signatures that would be detected at the two spacecraft for each configuration. The two ISEE spacecraft are assumed to be located at points A and B.

Magnetopause expansions or contractions or magnetopause surface waves would produce different signatures at the two spacecraft, as indicated on the right of the figure. The innermost spacecraft would be in the magnetospheric (high field) region for longer durations. As drawn, the outer spacecraft would detect high fields only when the inner spacecraft is also within the high-field region.

Propagating or convecting magnetosheath structures will have a much different signature. If the structure is relatively unchanging with time, and the spacecraft separation is small compared with the characteristic scale of the structure, the

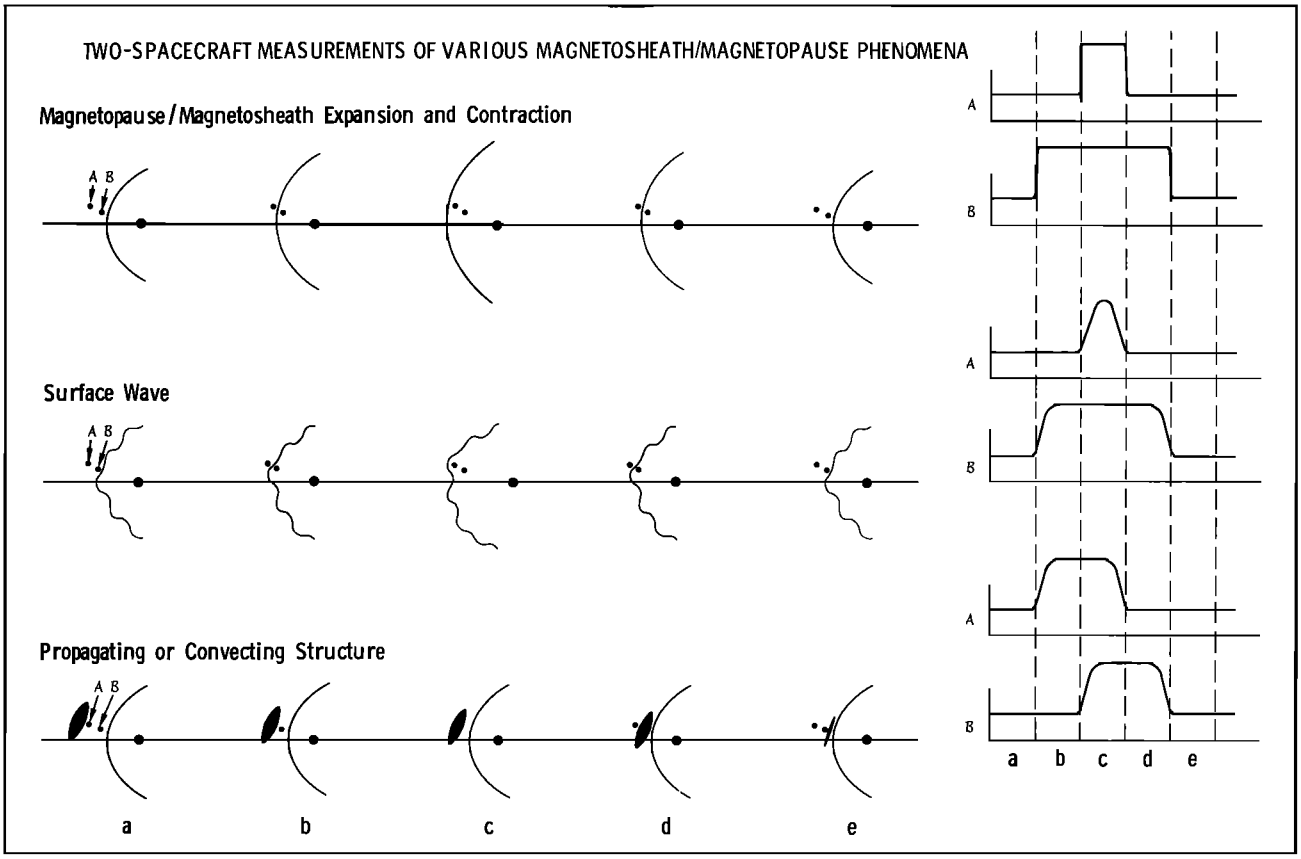

Fig. 9. The two-spacecraft signature of various magnetopause/near-magnetopause phenomena. The following phenomena are illustrated: radial motion of the magnetopause (top), surface waves on the magnetopause (center), and convecting/propagating magnetosheath structures (bottom). The two spacecraft are indicated as A and B. A time sequence of the motion is illustrated from a to e. The magnetic signatures at the two spacecraft corresponding to the time sequences are shown on the right of the figure. Of the three phenomena, only the propagating/convecting structure (bottom panel) gives a temporally offset, identical signature at the two spacecraft. The amount of offset is dependent on the convection/propagation velocity, the spacecraft separation, and the spatial shape of the magnetic structures.

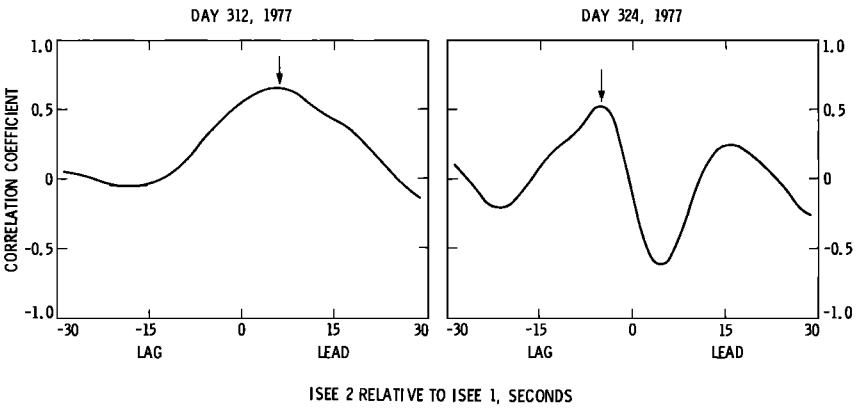

Fig. 10. Cross-correlation analyses of ISEE 1 and 2 magnetic field magnitude data for the events on day 312, 1977, and day 324, 1977. On day 312, the maximum correlation coefficient is detected when ISEE 2 leads ISEE 1 by 6 s. On day 324, the maximum correlation occurs when ISEE 1 leads ISEE 2 by 5 s.

two spacecraft will detect almost identical features, but offset in time.

From the comparison of the ISEE 1 and 2 day 324 data sets in Figure 8, it is evident that the magnetic oscillations are nearly static magnetosheath features that are convecting/propagating past the two spacecraft. The magnetic structures detected at the two spacecraft are nearly identical but offset in time, and the widths of the structures are comparable. This corresponds to the bottom configuration of Figure 9. The magnetic structures are first detected by ISEE 1, the outermost spacecraft, and then slightly later in time by ISEE 2. Thus the magnetic structures are convecting/propagating toward the magnetopause.

'Wavelength' Determination

The time delay for the magnetic structure to convect from one spacecraft to the other can be determined by performing cross-correlation analyses of the two data sets. The delay is determined most accurately by analyzing the high-time resolution magnetic field data. The results for the two intervals examined in this paper are shown in Figure 10. The parameter of interest is the time delay (lag) corresponding to the maximum positive correlation coefficient. On day 312, 1977, ISEE 2 leads ISEE 1 data by 5.8 s, whereas on day 324, 1977, ISEE 1 leads by 5.0 s. These values will be compared with those resulting from plasma convection.

Figure 11 gives the relative spacecraft locations, the magnetic field orientations, and the magnetosheath convection velocities. The last quantity is determined from three-dimensional electron distributions. These parameters are shown for both days 312 and 324. The figure corresponds to a projection of the above quantities into the ecliptic plane in solar ecliptic (SE) coordinates, since x is positive upward (toward the sun), y is positive to the left, and z is positive out of the paper. The values in the figure will be used to calculate the time delay for magnetosheath structures to be convected between the two spacecraft.

The two-dimensional geometry that enters the calculations is shown at the bottom of Figure 11. The field and plasma are convected in a direction, v_c, from spacecraft II to spacecraft I through a distance, L. The time delay is $L/v_c \cos \theta_{vc}$. From the figure the various angles are related: $\alpha + 180° + \phi_B = \phi_{II}$, where ϕ_B and ϕ_{II} are the azimuthal angles of the magnetic field and spacecraft II, respectively. To solve for τ, a geometrical relationship is used: $d = r \sin \alpha$, where r is the distance between the two spacecraft. Another angular identity is $\delta + 90° + \phi_B = \phi_v$, which can be substituted into the equation $L = d/\cos \delta$. ϕ_v is the azimuth angle of the convection velocity vector. From the above expressions it can be shown that the convection time is $\tau = r \sin (\phi_{II} - \phi_B - 180°)/v_c \cos (\phi_v - \phi_B - 90°) \cos \phi_{vc}$.

The time delays associated with magnetosheath convection from one spacecraft to the other have been calculated using the above equations. For day 312 the delay should be 10.4 s with the ISEE 2 data leading the ISEE 1 data. For day 324 the expected delay is 3.1 s, with the ISEE 1 data leading. The sign of the delay, depending on whether ISEE 1 leads or lags ISEE 2, is in agreement with the cross-correlation results. For comparison, the corresponding delays based on correlation analysis are 5.8 and 5.0 s, respectively.

The separation of the magnetic structures in the ecliptic plane can be determined by referring to Figure 11. The separation λ is equal to $T_w v_c \cos \theta_{vc} \cos \delta$ where T_w is the quasi-period of the structures and $v_c \cos \theta_{vc}$ is the convection velocity in the ecliptic plane. Using values of $T_w \simeq 50$ s for day 312 and $\simeq 21$ s for day 324, values of $\lambda = 1540$ km and 1630 km are found. Expressing the scale in proton gyroradii, the 'perpendicular' scale is $\sim 20\ \rho^+$ for 175-V ($T_p = 2 \times 10^6$ K) protons.

Three-Dimensional Analysis

The above two-dimensional calculation indicated an approximate scale size of the MHD structures in the direction of magnetosheath convection. The agreement between the expected delay between detecting the structures at ISEE 1 and 2 had the correct sense and the approximately correct delay times. To improve upon these results, the orientation (or shape) of the structures in three dimensions must be determined. In the case of planar waves, the orientation, or normal, is needed. For other possible structures, such as plasma tubes, both the shape and size must be determined.

Several attempts to determine the normals were made by applying the variance techniques of *Siscoe and Suey* [1972] to the high-resolution magnetic fields of ISEE 1 and 2. Unfortunately, because of the almost purely compressive nature of the waves in these events (very little angular change in the field), the results had large uncertainties associated with them. Normals could not be accurately

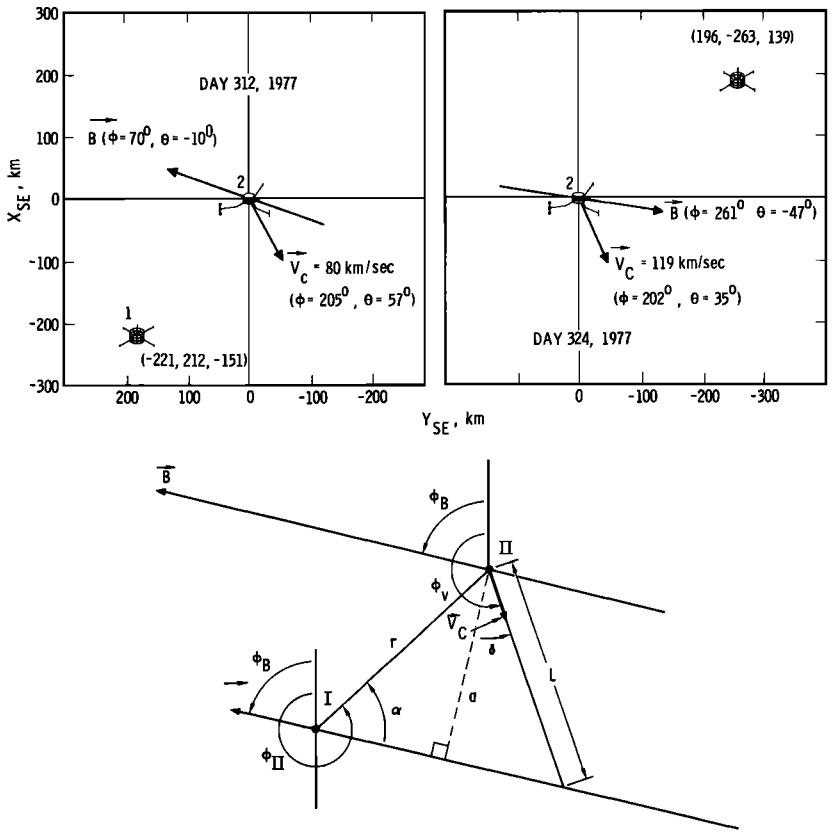

Fig. 11. The ISEE 1, 2 spacecraft relative location, the magnetosheath magnetic field orientation, and the magnetosheath plasma convection velocity for the events on days 312 and 324. ISEE 2 (denoted by a II) is at the origin of the solar ecliptic (SE) or spacecraft coordinate system. The positive x axis is upward (toward the sun), positive y is toward the left (dusk), and positive z is up out of the paper. The angles are defined in the conventional sense. The bottom panel is a schematic used to calculate the convection/propagation time of the field and plasma from one spacecraft to the other. The time delay is $\tau = r \sin(\phi_{II} - \phi_B - 180°)/v_c \cos(\phi_v - \phi_B - 90°) \cos\theta_{vc}$, for the above configuration. The distance between the two spacecraft is r, and ϕ_{II}, ϕ_B, and ϕ_v are the azimuthal angles of spacecraft II relative to spacecraft I, the magnetic field orientation, and the convection (and/or propagation) speed, respectively.

determined using the fields alone. Further knowledge of the three-dimensional shape of these structures must await either the selection of a more favorable wave data set or the use of the velocity and magnetic field and the inclusion of the dc electric field into the study.

Wave Normal Determination

Although the normal cannot be accurately determined from the magnetic field data alone, the direction relative to the ambient field can be inferred by the examination of the changes in the field direction and magnitude.

The geometry associated with the wave having a large-amplitude **b** propagating at an angle χ to the ambient field $\mathbf{B}_0$ is shown in Figure 12. It has been assumed that the structure is planar so that the field vectors, $\mathbf{B}_0$, $\mathbf{B}_1$ (one extreme in deflection angle corresponding to the minimum field magnitude), and $\mathbf{B}_2$ (corresponding to the maximum field magnitude), as well as **b** and **k**, all lie in the plane of the diagram.

From the three known parameters, $\mathbf{B}_1$, $\mathbf{B}_2$, and Ψ (the angular deflection in the field), and trigonometric relations, the following parameters can be derived:

$$b^2 = (B_1^2 + B_2^2 - 2B_1B_2 \cos\Psi)/4$$

$$B_0^2 = (B_1^2 + B_2^2)/2 - b^2$$

$$\chi = \cos^{-1}(b_z/b) \text{ or } \sin^{-1}[(B_2^2 - B_1^2)/4B_0b]$$

In the last expression, b_z is the component of the wave perturbation field perpendicular to B_0. For the waves appearing in Figure 2, $B_1 = 17$ nT, $B_2 = 32$ nT and $\Psi \cong 20°$. The above relations imply $b = 8.5$ nT, $B_0 = 24.2$ nT and $\chi = 63.3°$. An examination of different periods within this day

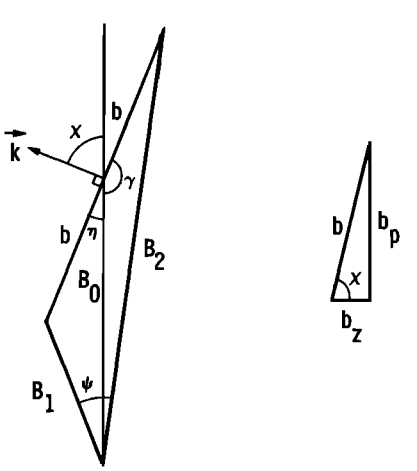

Fig. 12. Determination of the normal direction to the MHD structures. The minimum and maximum fields, $\mathbf{B}_1$ and $\mathbf{B}_2$, and the inclusive angle Ψ, are the measurable values. The wave perturbation vector **b** and the normal direction **k** are shown in the figure.

indicates that typical values of χ are 60°–70°. The drift mirror waves on day 312, 1977, have also been analyzed. The normals are directed at angles χ = 72°–82°. Thus the normals to the MHD structures are within 8°–30° of the direction perpendicular to B_0.

5. Drift Mirror Waves: Background

Prior studies have indicated the presence of compressive MHD structures in the earth's magnetosheath. Large-amplitude compressional wavelike structures were detected in the magnetosheath by the Mariner 4 magnetometer [*Siscoe et al.*, 1967]. Other examples of such magnetic structures, including power spectra, were obtained by *Fairfield and Ness* [1970] and *Fairfield* [1976]. In the spacecraft frame of reference, the compressive waves had periods of ~20 s. *Kaufmann et al.* [1970], using Explorer 12 magnetic field and $E > 200$ eV electron measurements, demonstrated that electron flux increases occurred and were out of phase with magnetic field enhancements. The authors concluded from the observed anticorrelation between field and plasma that the MHD structures were probably slow mode waves. Because such structures have not been observed in the interplanetary medium [*Coleman*, 1967; *Heppner et al.*, 1967; *Siscoe et al.*, 1968; *Unti and Neugebauer*, 1968; *Belcher et al.*, 1969], *Kaufmann et al.* [1970] and *Kaufmann and Horng* [1971] reached the conclusion that the MHD waves were generated at the bow shock or within the magnetosheath, with the most likely source being the mirror instability [*Chandrasekhar et al.*, 1958] in the outer magnetosheath.

Wave growth via the mirror instability occurs when $\beta_\perp/\beta_\parallel > 1 + 1/\beta_\perp$ [*Chandrasekhar et al.*, 1958; *Hasegawa*, 1969]. *Crooker et al.* [1976, 1979] have examined the earth's magnetosheath plasma and have determined that conditions for instability ($\beta_\perp/\beta_\parallel > 1.13$ for a typical magnetosheath plasma) is a persistent feature in the subsolar region.

Several physical processes are believed to be the cause of such an anisotropy. Preferential plasma heating (perpendicular to **B**) occurs as the solar wind passes through a perpendicular bow shock [*Kennel and Sagdeev*, 1967; *Kennel*, 1981]. Closer to the magnetopause, the compression of the draped magnetosheath fields [*Fairfield*, 1967] and the squeezing of the plasma along field lines [*Midgley and Davis*, 1963; *Zwan and Wolf*, 1976] will further reduce $P_\parallel/P_\perp$. *Crooker and Siscoe* [1977] expanding on the work of *Zwan and Wolf* [1976], demonstrated that the latter effect alone can create the necessary conditions for instability almost everywhere in the magnetosheath.

Hasegawa [1969, 1975] has made important advances in the understanding of the structure of the MHD waves associated with the (drift) mirror instability. Assuming the presence of a cold plasma, he demonstrated that the slow mode will be heavily Landau damped. Although the effect of 'warm' 200-eV magnetosheath plasma has not been studied yet, it is believed that strong Landau damping will also occur in the magnetosheath (A. Hasegawa and C. S. Lin, personal communication, 1982). By allowing an anisotropic plasma temperature and applying the Vlasov equation, a fourth MHD mode was discovered (in addition to the fast, Alfven, and slow modes). Hasegawa has shown that the drift mirror instability corresponds to a purely imaginary frequency and arises for almost perpendicular propagation ($k_\parallel/k_\perp$ small). Since ω is imaginary, the mode is nonoscillatory, corresponding to ever-growing 'blobs' of plasma. The spatial separation of the plasma blobs is predicted to correspond to the scale for maximum growth rate, roughly the proton gyroradius.

6. Nonoscillatory Drift Mirror Waves: Conclusions and Discussion

The magnetosheath MHD structures have many features which are properties of slow mode magnetoacoustic waves propagating at large angles to the ambient magnetic field. The structures are almost completely compressive (little or no field angular changes) and the plasma pressure is 180° out of phase with the magnetic pressure (Figures 4, 7). The normals to the structures are oriented at large angles (60°–80°) relative to the ambient magnetic field. For slow mode waves, the phase velocity is

$$V_{ph} = 1/2[(C_S^2 + C_A^2 + 2C_SC_A \cos\alpha)^{1/2} - (C_S^2 + C_A^2 - 2C_SC_A \cos\alpha)^{1/2}]$$

where α is the angle of propagation with respect to the magnetic field, C_S is the sound speed $(\gamma P_0/\rho_0)^{1/2}$, and C_A is the Alfven speed [*Landau and Lifshitz*, 1960; *Kantrowitz and Petschek*, 1966]. For magnetosheath values of $T_p = 2 \times 10^6$ K, $T_e = 3 \times 10^5$ K, $\gamma = 2$ [*Zhuang and Russell*, 1981], C_S = 210 km/s, and C_A = 75 km/s. Substituting into the above expression to determine the speed, it is found that the slow mode velocity for the illustrated examples would be less than the magnetosheath convection speed (25–70 km/s for α = 80° to 60° in comparison to V_c = 80–119 km/s). Thus the observation that the propagation time delays between the two spacecraft can be explained by convection alone can also be consistent with the structures being slow mode waves.

However, the variations of the electron and proton temperature and temperature anisotropies as functions of low-field (high β) and high-field (low β) regions are clearly inconsistent with the structures being slow mode waves. Both the electron and proton temperatures are consistently higher (by 5–10%) in the low-field regions. The electron perpendicular temperature, $T_\perp{}^-$, is almost always greater than $T_\parallel{}^-$, with the largest value of temperature anisotropy, $T_\perp{}^-/T_\parallel{}^-$, detected in the low-field regions. For the protons, all of the measurements studied gave values of $T_\perp{}^+/T_\parallel{}^+ > 1$. To first order, the proton temperature anisotropy is roughly constant. (A consistent picture of the proton temperature anisotropy dependence on high and low β regions was not obtained—this feature of the drift mirror waves is currently being investigated in greater detail.) A final point is that the temperature anisotropies have a very narrow range in values: $0.9 \leq T_\perp{}^-/T_\parallel{}^- \leq 1.2$ and $1.06 \leq T_\perp{}^+/T_\parallel{}^+ \leq 1.2$, much less than the variation in the magnetic field magnitude (greater than or equal to a factor of 2).

All of the above features indicate that the low-field and high-field regions are adiabatically decoupled. Conservation of the first adiabatic invariant ($kT_\perp/B$) would imply lower plasma temperatures in the low-field regions than in the high-field regions, opposite to the observations. The temperature anisotropies would also be expected to decrease significantly within the low-field regions, again contrary to the observations.

On the other hand, the properties of the MHD structures determined in this paper are consistent with their being

nonoscillatory drift mirror 'waves.' The anticorrelation between the plasma pressure and field pressure and the constant total pressure are predicted by theory. Assuming bi-Maxwellian distributions, *Hasegawa* [1969] derived the pressure terms for the drift mirror waves: $P_\perp \simeq 2mn_0v_\perp{}^2$ $(1 - T_\perp{}^+/T_\parallel{}^+)B_z/B_0$ and $P_\parallel = mn_0v_\parallel{}^2(1 - T_\perp{}^+/T_\parallel{}^+)B_z/B_0$ (equations (60) and (61)). For $T_\perp{}^+/T_\parallel{}^+ > 1$ (as in the cases presented here; see also *Crooker et al.* [1979]), both the parallel and perpendicular plasma pressures will oscillate out of phase with the magnetic field, as is observed. Because these are nonoscillatory structures, once created, the drift mirror 'waves' will evolve independently as they are compressed and convected toward the magnetopause.

The quasi-periodic spacing between plasma blobs was determined to be $\sim 20\ \rho^+$ in the plasma rest frame. This is somewhat larger than the theoretical estimate of $\sim 1\rho^+$ but is still in reasonable agreement.

Because the conditions for the mirror instability are so easily met, one would expect to find these MHD waves in the magnetosheaths of other planets. This is particularly true for the outer planets. The tightly wound Parker interplanetary magnetic field spiral [*Thomas and Smith,* 1980] at large distances will lead to shocks which are quasi-perpendicular near the subsolar regions. The consequential magnetosheath pressure anisotropies created at the shocks [*Kennel and Sagdeev,* 1967] and the further plasma compression described by *Zwan and Wolf* [1976] would be expected to lead to instability.

A striking example of large amplitude compressional field oscillations is found in the Pioneer 11 observations of Jupiter, in Figure 13. The field is in solar-interplanetary coordinates. In this system, the longitude angle increases from the sun-spacecraft line ($\hat{R}$) toward the $-\hat{R} \times \hat{\Omega}_s$ (or $\hat{T}$) direction, where $\hat{\Omega}_s$ is the solar rotation axis. θ is the colatitude angle out of the $\hat{R}$-$\hat{T}$ plane. The field lies in the ecliptic plane and is nearly orthogonal to the Jupiter-sun line. The magnetic oscillations are almost completely compressional with the little variations observed in either the ϕ or θ angles. An approximate spacing between the field maxima is ~300 s. With a magnetic field magnitude of 2 nT, this would correspond to a scale size of $25\rho^+$ assuming the same magnetosheath convection speed and proton thermal temperatures as at ISEE.

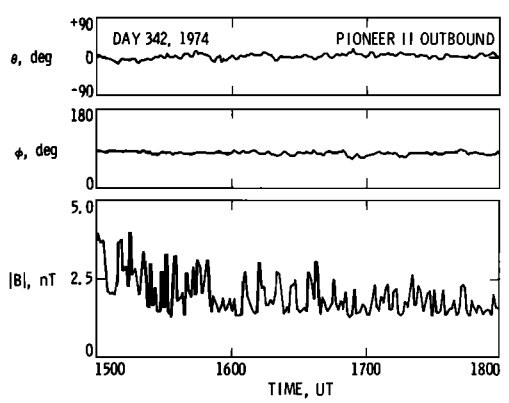

Fig. 13. An example of compressional magnetic structures detected in the Jovian magnetosheath. During this event, Pioneer 11 was close to the subsolar point at 88 R_J and 1140 local time. The field is plotted in solar-interplanetary (SI) coordinates. The magnetic field variations are almost purely compressional with little or no accompanying directional changes. The spacing between field maxima is ~300 s, or $25\rho^+$, similar to the observations at the earth.

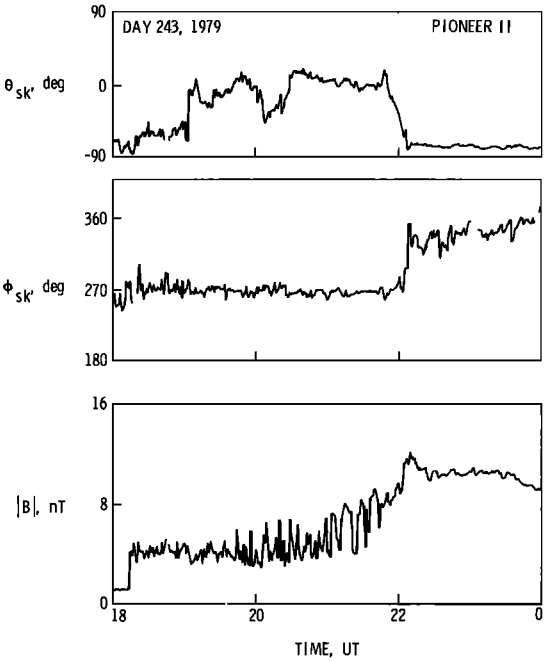

Fig. 14. An example of compressional magnetic structures in the Saturnian magnetosheath [from *Smith et al.,* 1980]. Pioneer 11 is at 1155 local time and a radial distance of 18 R_S. The bow shock crossing occurs shortly after 1800 UT. The magnetopause appears as an abrupt change in the longitude and latitude angles accompanied by a maximum in field strength just after 2200 hours. The magnetosheath is characterized by a gradually increasing average field magnitude and large pulsations between 2000 and 2200 hours. The magnetic oscillations are almost totally compressional. The spacing between magnetic peaks is approximately 250 s. This is consistent with $\sim 40\ \rho^+$ scale sizes, similar to that observed at earth.

Figure 14 is an example of compressional magnetic structures in the Saturnian magnetosheath, taken from *Smith et al.* [1980]. Pioneer is at 1155 local time and a radial distance of 18 R_S. The bow shock crossing occurs shortly after 1800 UT. The magnetopause appears as an abrupt change in the longitude and latitude angles accompanied by a maximum in field strength just after 2200 UT. There are large magnetic field magnitude oscillations present throughout the magnetosheath, particularly between 2000 and 2200 UT. The spacing between field maxima is approximately 250 s. Using a field strength of 4 nT, these structures would have a scale of $40\rho^+$, if the convection speed and temperatures are similar to the cases at earth. The magnetic field properties of the oscillations in the Saturnian and Jovian magnetosheaths have been examined to determine if substructure exist. None were found within the limits of the instrument digital resolution of 0.015 nT and 0.05 nT, respectively.

The scale sizes of the magnetic structures in terms of the local proton gyroradius are approximately constant, in agreement with theory [*Hasegawa,* 1975]. Thus this physical process may be a common feature of the solar wind interaction with the planets (similar field buildup and plasma depletion has been observed at Venus [*Russell et al.,* 1979]) and, as such, deserved further study.

The consequences of the presence of nonoscillatory drift mirror 'waves' in planetary magnetosheaths have not yet been explored. If the theoretical modelling of *Zwan and Wolf*

[1976] and *Hill* [1975] is correct, the convection of these waves to the magnetopause may have important implications for magnetic reconnection. The drift mirror instability will cause increasing plasma depletion, leaving high-field, low β regions. However, at the same time, the high β regions will be composed of plasma with an anisotropy ($P_\perp/P_\parallel > 1$) which is conducive for reconnection [*Hill*, 1975]. The existence of the nonoscillatory drift mirror 'waves' near the magnetopause may thus lead to patchy, sporadic reconnection.

7. Interrelationship Between Lion Roars and Drift Mirror Waves

Besides having common sources of free energy, lion roars and drift mirror waves may be intimately coupled in another way. The high β plasma regions of the MHD waves can also act as wave guides, causing lion roars to be confined to propagate along the longitudinal extent of the blobs (parallel to the magnetic field). Lion roars have a phase velocity c/n, where the index of refraction is given by $n = [4\pi Ne^2/m^-\omega(\Omega^- \cos\theta - \omega)]^{1/2}$. As demonstrated in Figure 4, the high β regions have plasma enhancements of 25–50%. Thus gradients of these regions are also gradients in the wave index of refraction. For modest wave propagation angles to the magnetic field and for wave frequencies $<0.5\ \Omega^-$ (both features are characteristic of lion roars [*Smith and Tsurutani*, 1976]), the lion roars will be internally reflected and will be confined to the density 'ducts' [*Helliwell*, 1965]. Moreover, recent calculations by *Calvert* [1982] have demonstrated that whistler mode wave can also be ducted by magnetic field variations in a manner analogous to density ducting. For the drift mirror waves, both effects will work in concert and will lead to strong lion roar confinement to the high β, low-field regions.

If lion roars are being confined to propagate within the plasma ducts elsewhere in the magnetosheath, the typical ~1–2 second lion roar durations may be due to the convection of these MHD structures (containing lion roars) past the spacecraft. For a typical flow velocity of ~200–300 km/s and lion roar (and depressed field) durations of 1–2 s, a 'duct' scale size is 150–300 km or 1–2 proton gyroradii. This is in good agreement with the scale for maximum growth rate indicated by *Hasegawa* [1975], and may represent a growing drift mirror wave.

The plasma ducting of the lion roars and the strong Landau damping for wave angles >20° to the magnetic field [*Thorne and Tsurutani*, 1981] will confine lion roars to propagate along the magnetic field in the direction of the duct extensions. The lion roar group velocity is quite large ($\sim 3 \times 10^8$ cm/s) and thus lion roars will rapidly propagate to the extremities of the tubes. Calculations [*Thorne and Tsurutani*, 1981] indicate that the wave damping will then become a significant factor, and the waves will not be able to propagate more than a fraction of an R_E beyond the MHD high β structures. The propagation of lion roars out the ends of the high β portions of the drift mirror waves is one possible explanation of the emissions that are not associated with magnetic field decreases [*Smith and Tsurutani*, 1976].

It is also possible that plasma conditions in other regions of the magnetosheath may be conducive for the growth of lion roars, independent of the drift mirror instability. In the example shown in this paper, the high magnetic field strengths found close to the magnetopause ordinarily inhibit emission growth because of the correspondingly high resonant energies (>100 eV). It is only because of the onset of the drift mirror instability and the corresponding local reduction of the critical energy that the electron cyclotron instability occurs, leading to the remarkable correlation between the lion roars and drift mirror 'waves' shown in this paper. On the other hand, in the flanks of the magnetosheath where the field and plasma compression are modest (B = 10 nT, N = 10/cm^3), the resonant energy is reasonably low (~18 eV) and the (theoretical) required anisotropy for generating ~100 Hz waves is only $A^- \geq 0.5$. Immediately behind the subsolar point of the bow shock (B = 15 nT, N = 20/cm^3), 200-Hz emissions can be generated for anisotropies of $\simeq$0.9. Thus it is possible that lion roars may be generated in other regions of the magnetosheath by the electron cyclotron instability without the aid of the drift mirror instability. This question can only be answered by a careful statistical study to determine the relationship between lion roars and the drift mirror instability in all regions of the magnetosheath.

To date, only a limited amount of magnetosheath data has been analyzed. The authors are currently studying lion roars and MHD structures in different regions within the magnetosheath and for a variety of interplanetary conditions to determine if the results presented in this article are representative of all lion roars. As one example of a test of the model, the necessary pressure anisotropies for the growth of both lion roars and the drift mirror waves would not be expected in the magnetosheath behind parallel shocks (nominally ~1000 local time). Thus the determination of the local time dependence of lion roar occurrence will improve our understanding of the generality of the results presented in this paper. Additionally, simultaneous plasma and fields at Jupiter and Saturn may be analyzed to determine if the magnetic features reported in this paper are indeed drift mirror instability waves and, if so, to determine whether the same interrelationship between lion roars and the drift mirror waves are found at these distant planets.

Acknowledgments. This work was initiated and supported under the ISEE Guest Investigator Program. Discussions with numerous people were helpful in the interpretation of the MHD structures and the drift mirror instability. We wish to thank A. Hasegawa, R. L. Kaufmann, N. U. Crooker, B. E. Goldstein, C. T. Russell, and R. M. Thorne for the useful conversations that we had with them. C. T. Russell kindly supplied the magnetic field data. K. Choate and R. Okida helped with the computer programming and figure preparation. This paper represents one aspect of research done at the Jet Propulsion Laboratory, California Institute of Technology, for NASA under contract NAS7-100. The Los Alamos portion of this work was carried out under the auspices of the U.S. Department of Energy with NASA support under contract S-50864A. This research was also supported by contract NAS5-20093 with the University of Iowa.

The Editor thanks D. H. Fairfield and R. W. Fredricks for their assistance in evaluating this paper.

References

Anderson, R. R., C. C. Harvey, M. M. Hoppe, B. T. Tsurutani, T. E. Eastman, and J. Etcheto, Plasma waves near the magnetopause, *J. Geophys. Res., 87*, 2082, 1982.

Bame, S. J., J. R. Asbridge, H. E. Felthauser, J. P. Gore, G. Paschmann, P. Hemmerich, K. Lehmann, and H. Rosenbauer, ISEE-1 and ISEE-2 fast plasma experiment and the ISEE-1 solar wind experiment, *IEEE Trans. Geosci. Electron., GE-16*, 216, 1978.

Belcher, J. W., L. Davis, Jr., and E. J. Smith, Large-amplitude Alfven waves in the interplanetary medium: Mariner 5, *J. Geophys. Res., 74*, 2302, 1969.

Calvert, W., Whistler ducting by a spatial variation of magnetic field strength, *J. Geophys. Res.*, in press, 1982.

Chandrasekhar, S. A., A. N. Kaufman, and K. M. Watson, The stability of the pinch, *Proc. R. Soc. London Ser. A, 245*, 435, 1958.

Coleman, P. J., Jr., Wavelike phenomena in the interplanetary plasma: Mariner 2, *Planet. Space Sci., 15*, 953, 1967.

Crooker, N. U., and G. L. Siscoe, A mechanism for pressure anisotropy and mirror instability in the dayside magnetosheath, *J. Geophys. Res., 82*, 185, 1977.

Crooker, N. U., G. L. Siscoe, and R. B. Geller, Persistent pressure anisotropy in the subsonic magnetosheath region, *Geophys. Res. Lett., 3*, 65, 1976.

Crooker, N. U., T. E. Eastman, and G. S. Stiles, Observations of plasma depletion in the magnetosheath of the dayside magnetopause, *J. Geophys. Res., 84*, 869, 1979.

Fairfield, D. H., The ordered magnetic field of the magnetosheath, *J. Geophys. Res., 72*, 5865, 1967.

Fairfield, D. H., Magnetic fields of the magnetosheath, *Rev. Geophys. Space Phys., 14*, 117, 1976.

Fairfield, D. H., and N. F. Ness, Magnetic field fluctuations in the earth's magnetosheath, *J. Geophys. Res., 75*, 6050, 1970.

Gurnett, D. A., F. L. Scarf, R. W. Fredricks, and E. J. Smith, The ISEE-1 and ISEE-2 plasma wave investigation, *IEEE Trans. Geosci. Electron., GE-16*, 225, 1978.

Hasegawa, A., Drift mirror instability in the magnetosphere, *Phys. Fluids, 12*, 2642, 1969.

Hasegawa, A., *Plasma Instabilities and Nonlinear Effects, Phys. and Chem. in Space 8*, p. 94, Springer-Verlag, New York, 1975.

Helliwell, R. A., *Whistlers and Related Ionospheric Phenomena*, p. 43, Stanford University Press, Stanford, Calif., 1965.

Heppner, J. P., M. Sugiura, T. L. Skillman, B. G. Ledley, and M. Campbell, OGO-A magnetic field observations, *J. Geophys. Res., 72*, 5417, 1967.

Hill, T. W., Magnetic merging in a collisionless plasma, *J. Geophys. Res., 80*, 4689, 1975.

Kantrowitz, A. R., and H. E. Petschek, MHD characteristics and shock waves, in *Plasma Physics and Shock Waves*, edited by W. B. Kunkel, 147 pp., McGraw-Hill, New York, 1966.

Kaufmann, R. L., and J.-T. Horng, Physical structure of hydromagnetic disturbances in the inner magnetosheath, *J. Geophys. Res., 76*, 8189, 1971.

Kaufmann, R. L., J.-T. Horng and A. Wolfe, Large-amplitude hydromagnetic waves in the inner magnetosheath, *J. Geophys. Res., 75*, 4666, 1970.

Kennel, C. F., Collisionless shocks and upstream waves and particles: Introductory remarks, *J. Geophys. Res., 86*, 4325, 1981.

Kennel, C. F., and H. E. Petschek, Limit of stably trapped particle fluxes, *J. Geophys. Res., 71*, 1, 1966.

Kennel, C. F., and R. Z. Sagdeev, Collisionless shock waves in high plasmas, 1, *J. Geophys. Res., 72*, 3303, 1967.

Landau, L. D., and E. M. Lifshitz, *Electrodynamics of Continuous Media*, 213 pp., Pergamon, New York, 1960.

Midgley, J. E., and L. Davis, Jr., Calculation by a moment technique of the perturbation of the geomagnetic field by the solar wind, *J. Geophys. Res., 68*, 5111, 1963.

Ogilvie, K. W., J. D. Scudder, and H. Doong, The electron spectrometer experiment on ISEE-1, *IEEE Trans. Geosci. Electron., GE-16*, 261, 1978.

Russell, C. T., The ISEE 1 and 2 fluxgate magnetometers, *IEEE Trans. Geosci. Electron., GE-16*, 239, 1978.

Russell, C. T., R. C. Elphic, and J. A. Slavin, Initial Pioneer Venus magnetic field results: Dayside observations, *Science, 203*, 745, 1979.

Siscoe, G. L., and R. W. Suey, Significance criteria for variance matrix applications, *J. Geophys. Res., 77*, 1321, 1972.

Siscoe, G. L., L. Davis, Jr., P. J. Coleman, Jr., E. J. Smith, and D. E. Jones, Shock-aligned magnetic oscillations in the magnetosheath: Mariner 4, *J. Geophys. Res., 72*, 5524, 1967.

Siscoe, G. L., L. Davis, Jr., P. J. Coleman, Jr., E. J. Smith, and D. E. Jones, Power spectra and discontinuities of the interplanetary magnetic field: Mariner 4, *J. Geophys. Res., 73*, 61, 1968.

Smith, E. J., and B. T. Tsurutani, Magnetosheath lion roars, *J. Geophys. Res., 81*, 2261, 1976.

Smith, E. J., R. E. Holzer, and C. T. Russell, Magnetic emissions in the magnetosheath at frequencies near 100 Hz, *J. Geophys. Res., 74*, 3027, 1969.

Smith, E. J., A. M. A. Frandsen, and R. E. Holzer, Lion roars in the magnetosheath (abstract), *Eos Trans. AGU, 52*, 903, 1971.

Smith, E. J., B. V. Connor, and G. T. Foster, Jr., Measuring the magnetic fields of Jupiter and the outer solar system, *IEEE Trans. Magn., 11*, 962, 1975.

Smith, E. J., L. Davis, Jr., D. E. Jones, P. J. Coleman, Jr., D. S. Colburn, P. Dyal, and C. P. Sonett, Saturn's magnetosphere and its interaction with the solar wind, *J. Geophys. Res., 85*, 5655, 1980.

Thomas, B. T., and E. J. Smith, The Parker spiral configuration of the interplanetary magnetic field, *J. Geophys. Res., 85*, 6861, 1980.

Thorne, R. M., and B. T. Tsurutani, Generation of magnetosheath lion roars, *Nature, 293*, 384, 1981.

Unti, T. W. J., and M. Neugebauer, Alfven waves in the solar wind, *Phys. Fluids, 11*, 563, 1968.

Zhuang, H. C., and C. T. Russell, An analytic treatment of the structure of the bow shock and magnetosheath, *J. Geophys. Res., 86*, 2191, 1981.

Zwan, B. J., and R. A. Wolf, Depletion of the solar wind plasma near a planetary boundary, *J. Geophys. Res., 81*, 1636, 1976.

(Received January 14, 1982;
revised April 29, 1982;
accepted April 30, 1982.)